analytical chemistry

pubs.acs.org/ac Article

Mini-Program Enabled IoT Intelligent Molecular Diagnostic Device for Co-Detection and Spatiotemporal Mapping of Infectious Disease Pathogens

Kaizheng Wang, Tao Zhang, Tianjiao Jiao, Feibiao Pang, Fengyi Dai, Zhanfang Zhang, Xiang Li, Yao Chen, Hongyu Zhang, Zhiguang Chen, and Jinzhao Song*

Cite This: *Anal. Chem.* 2024, 96, 13494−13503 Read Online

ACCESS | Metrics & More | Article Recommendations | Supporting Information

ABSTRACT: Effective detection of infectious pathogens is crucial for disease prevention and control. We present an innovative Internet of Things (IoT) molecular diagnostic device featuring a WeChat mini-program for simultaneous detection and spatiotemporal mapping of respiratory pathogens. Leveraging social software's widespread usage, our device integrates seamlessly with WeChat, eliminating the need for app downloads and installations. Through a comprehensive detection system, including a user-friendly mini-program, a portable Point-of-Care fluorescence detector, and a diagnostic information management platform (EzDx Cloud), we demonstrate high sensitivity and specificity in detecting common respiratory viruses. Our SARS-CoV-2/H1N1 combo test kit, developed using a novel one-tube/one-step loop-mediated isothermal amplification-CRISPR method, shows remarkable performance. We address challenges in at-home nucleic acid testing by providing a cost-effective solution capable of detecting multiple pathogens simultaneously. Our system's versatility accommodates various assays operating at different temperatures and fluorescence intensities, offering significant advantages over traditional methods. Moreover, integration with EzDx Cloud facilitates disease monitoring and early warning systems, enhancing public health management. This study highlights the potential of our IoT molecular diagnostic device in revolutionizing infectious disease detection and control, with wide-ranging applications in both human and animal population.

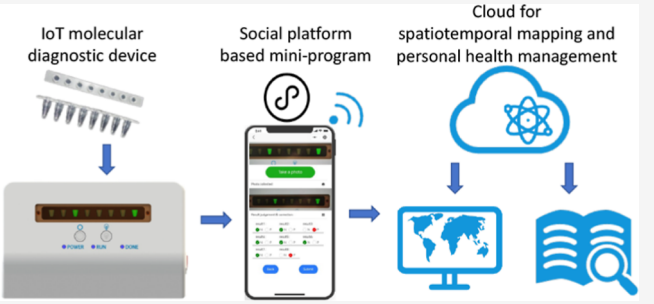

1. INTRODUCTION

In order to facilitate the rapid and widespread adoption of molecular diagnostics and enhance the effectiveness of infectious disease prevention and control, it is crucial for the diagnostic system to gain broad acceptance among the general public.[1,2] Social software, often referred to as social apps or social platforms, encompasses communication and interactive tools that are predominantly Internet-based. Popular examples include WhatsApp, WeChat, X (formerly known as Twitter), Facebook, and others, all of which have deeply penetrated users' daily lives. Mini-programs can be developed within these platforms, such as the WeChat mini-program, which seamlessly integrates into WeChat without requiring downloads or installations. Users can access these instant apps through various entry points, including the "Mini Programs nearby" feature, name-based searches, or by simply scanning a unique QR code. Notably, the development cost for WeChat mini-programs is relatively low when compared to native apps. Additionally, mini-programs offer the advantage of monitoring social interactions and collecting personal information with user permission, enhancing their utility in the context of diagnostics and prevention.

The timely detection of infectious diseases, particularly respiratory illnesses, serves as a critical linchpin for enabling early isolation, appropriate treatment, and effective containment measures. Even as COVID-19 has transitioned into a new phase characterized by the attainment of herd immunity,[3,4] the capacity to detect and differentiate respiratory pathogens remains of paramount importance. This capability assumes a pivotal role in the identification of COVID-19 cases and the distinction of influenza from other respiratory ailments.[5−7] In the case of influenza, Oseltamivir has demonstrated notable efficacy in controlling the replication of the influenza virus, proving effective against both type A and type B strains.[8] Notably, for individuals at higher risk, particularly children under the age of 2 diagnosed with severe influenza, the initiation of Oseltamivir treatment within 48 h of

Received: April 4, 2024
Revised: July 20, 2024
Accepted: July 25, 2024
Published: July 31, 2024

https://doi.org/10.1021/acs.analchem.4c01762
Anal. Chem. 2024, 96, 13494−13503

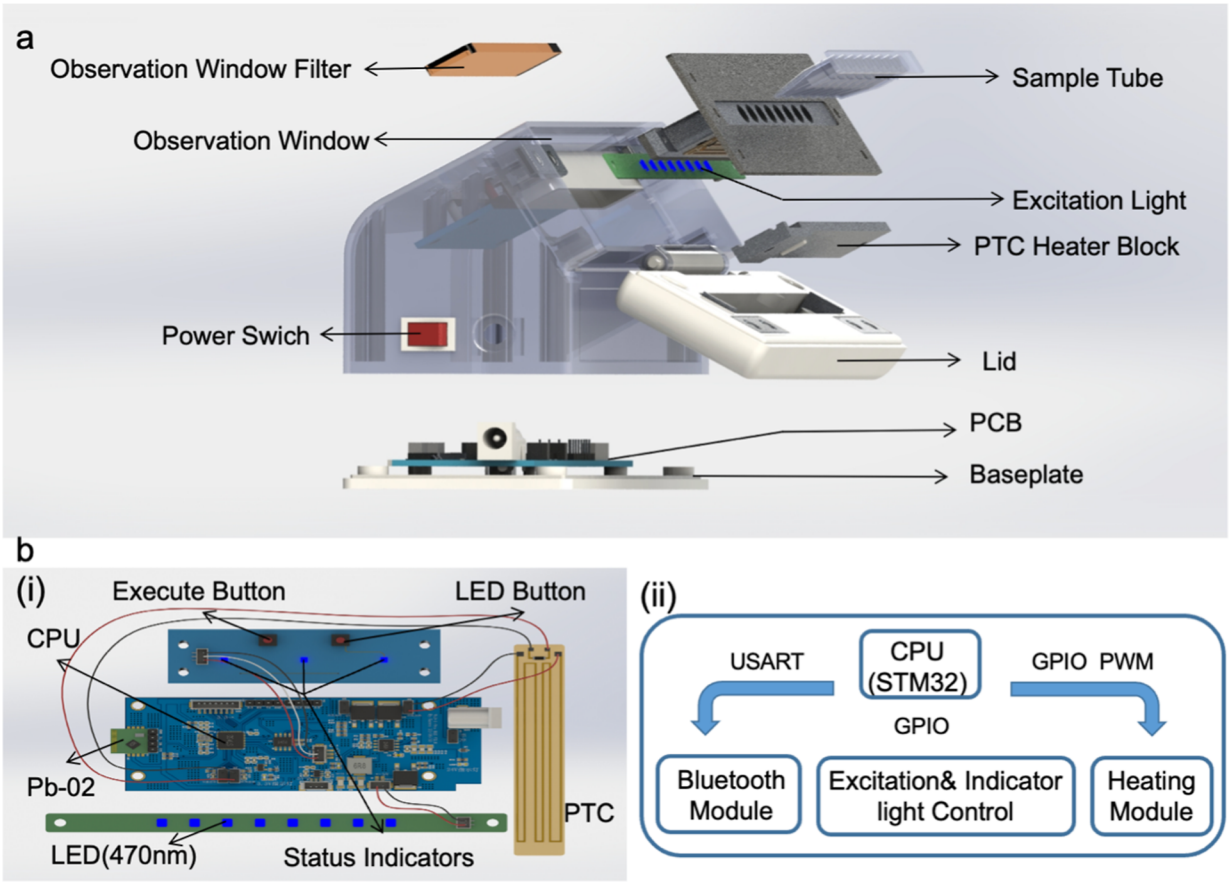

Figure 1. Device Structure and Hardware. (a) Structure of the equipment shell and its internal components. (b) PCB design and construction of hardware modules (i); MCU working principle and communication protocol (ii).

symptom onset yields substantial reductions in hospitalization and mortality rates while concurrently minimizing the risk of complications.[9,10]

At-home testing has become a valuable tool in the efforts to combat infectious disease.[11−14] It empowers individuals to promptly assess the cause of their symptoms without the necessity of clinical visits, thus diminishing the risk of transmission within healthcare settings. Furthermore, it facilitates the prompt implementation of self-isolation measures when needed. In the context of at-home testing, nucleic acid testing offers several distinct advantages when compared to antigen testing:[15−21] (1) it boasts higher sensitivity and specificity, rendering it more reliable for detecting asymptomatic or mild cases of infection. (2) It can perform genotyping, allowing for the identification of critical variants.[22]

Nevertheless, despite these advantages, at-home nucleic acid testing encounters several challenges:[23] (1) the absence of cost-effective devices capable of simultaneously detecting various infectious pathogens remains a limitation.[24,25] (2) The per-test cost can be relatively high.[26] (3) Ensuring the accuracy of self-administered tests and interpreting results correctly poses an ongoing challenge. (4) Some at-home testing devices necessitate App downloads or installations, potentially diminishing the user experience and limiting their widespread adoption.

In this study, we have innovatively developed a WeChat mini-program enabled IoT (Internet of Things) molecular diagnostic device designed for the codetection and spatiotemporal mapping of infectious disease pathogens, with a focus on respiratory diseases to demonstrate the device's capabilities. Our comprehensive detection system incorporates several essential components, including a user-friendly WeChat mini-program, a cost-effective and portable point-of-care (POC) fluorescence detector, a combo test kit capable of identifying two prevalent respiratory viruses—SARS-CoV-2 (Severe Acute Respiratory Syndrome Coronavirus 2) and H1N1 (Influenza A virus subtype H1N1), and a diagnostic information management platform (EzDx Cloud). This platform features a spatiotemporal mapper tailored specifically for analyzing infectious disease epidemics and providing early warnings, along with a health/diagnostic information management system. Significantly, our SARS-CoV-2/H1N1 combo test kit was developed using our newly devised one-tube/one-step loop-mediated isothermal amplification (LAMP)-CRISPR method, which integrates LAMP with a recently discovered thermophilic Cas12b protein, demonstrating remarkable sensitivity and specificity for detecting common respiratory viruses.

2. MATERIALS AND METHODS

2.1. Development of a WeChat Mini-Program for Integrating Smartphone with IoT Molecular Diagnostic Device, Back-End Database, and Web Systems. *2.1.1. IoT Molecular Diagnostic Device.* We have developed a hand-held isothermal fluorescence detection device[27] that is simple, cost-effective, and efficient for one-pot/one-step LAMP-CRISPR visual detection. As shown in Figure 1a, this compact device features eight reaction wells designed to accommodate 0.2 mL

https://doi.org/10.1021/acs.analchem.4c01762
Anal. Chem. 2024, 96, 13494−13503

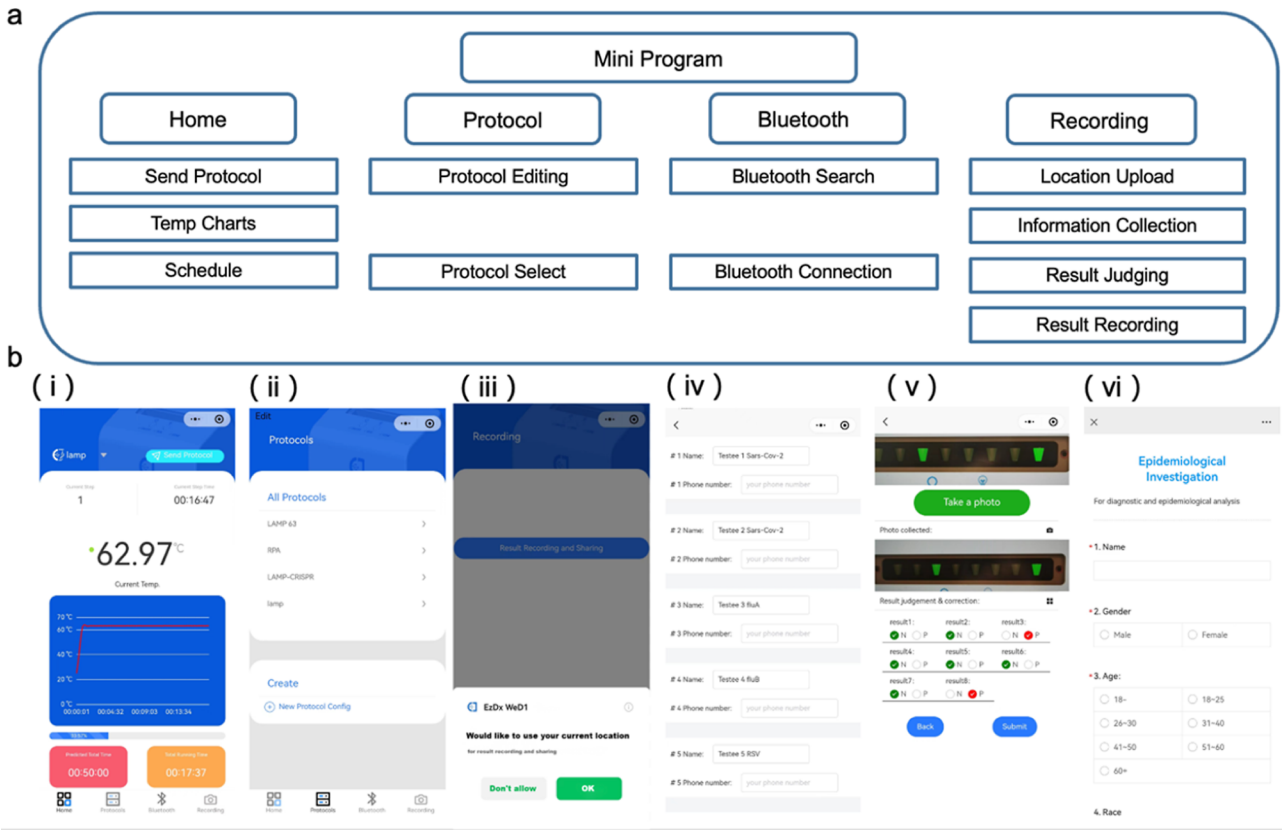

Figure 2. The WeChat mini-program. (a) Software architecture of the mini-program, which is divided into four different sections based on the UI design: home, protocol, bluetooth, recording, and questionnaire survey. (b) Screenshots of the mini-program interface, which include (i) home page, (ii) protocol setting page, (iii–v) result recording and sharing pages, and (vi) questionnaire survey page.

standard PCR tubes on an aluminum alloy heating block. The device's heating module is managed by a microcontroller (MCU) (Figure 1b), which effectively controls the heating process through GPIO (general-purpose input/output) in alignment with various heating profiles. Seamless data communication between the device and a smartphone mini-program is facilitated by a Bluetooth module, allowing for real-time monitoring of the reaction progress. The optical system features a 480 nm light-emitting diode (LED) light source that serves as the fluorescence excitation module. To manually trigger the LED for light excitation, an external GPIO button on the MCU (STM32) was used, while another GPIO button controlled the heating module in accordance with the preset reaction program. The observation window filter effectively blocks excitation light at 480 nm and allows for the passage of fluorescence signals within the range of 500 to 670 nm. This allows for direct visualization of the results of fluorescence detection via the naked eye, and for the results to be conveniently recorded and shared with the accompanying smartphone mini-program.

2.1.2. WeChat Mini–Program. Our diagnostic system's WeChat mini-program is built using the Uniapp framework, a lightweight Vue framework that offers compatibility with a variety of social media platforms. This framework allows developers to employ a single JavaScript codebase for deploying the mini-program across multiple social media platforms, provided the functions are mini-program-compatible. As illustrated in Figure 2, our mini-program includes all essential functions for device control and data collection, encompassing the Home, Protocols, Bluetooth, Recording pages, and Questionnaire survey (Figure 2b(i,ii)). Through the WeChat mini-program, users have the capability to edit, modify, and transmit amplification protocols (heating profiles) to the device's MCU, which are then securely stored within the device. This feature enhances user control and customization. Moreover, the mini-program exhibits exceptional compatibility with a broad spectrum of mobile devices, catering to different operating systems such as iOS and Android.

The distinctive nature of social media platforms simplifies the process of obtaining location and personal information, enhancing user-friendliness compared to traditional apps and streamlining the user authorization process. Upon receiving user authorization and consent, we gather location information from the user's mobile device and collect essential personal data, including the testee's name, phone number, test results, and other pertinent health-related information. The information acquisition process follows these key steps: after the user consents to our privacy policy, the system checks for location permissions (Figure 2b(iii)). In case of denial, the program prompts the user to grant location permissions. Once granted, the current location is obtained and stored locally. The user inputs the testee's name on the dedicated page and their mobile phone number for SMS notifications (Figure 2b(iv)). Following the information collection, users proceed to the photocapturing page to capture the test results (Figure 2b(v)). Once the mini-program automatically interprets the results, corrections can still be made manually and uploaded after confirmation. Finally, the mini-program enables users to jump to the epidemiological questionnaire survey (wjx.cn) that we designed, which includes necessary personal information (such

https://doi.org/10.1021/acs.analchem.4c01762
Anal. Chem. 2024, 96, 13494−13503

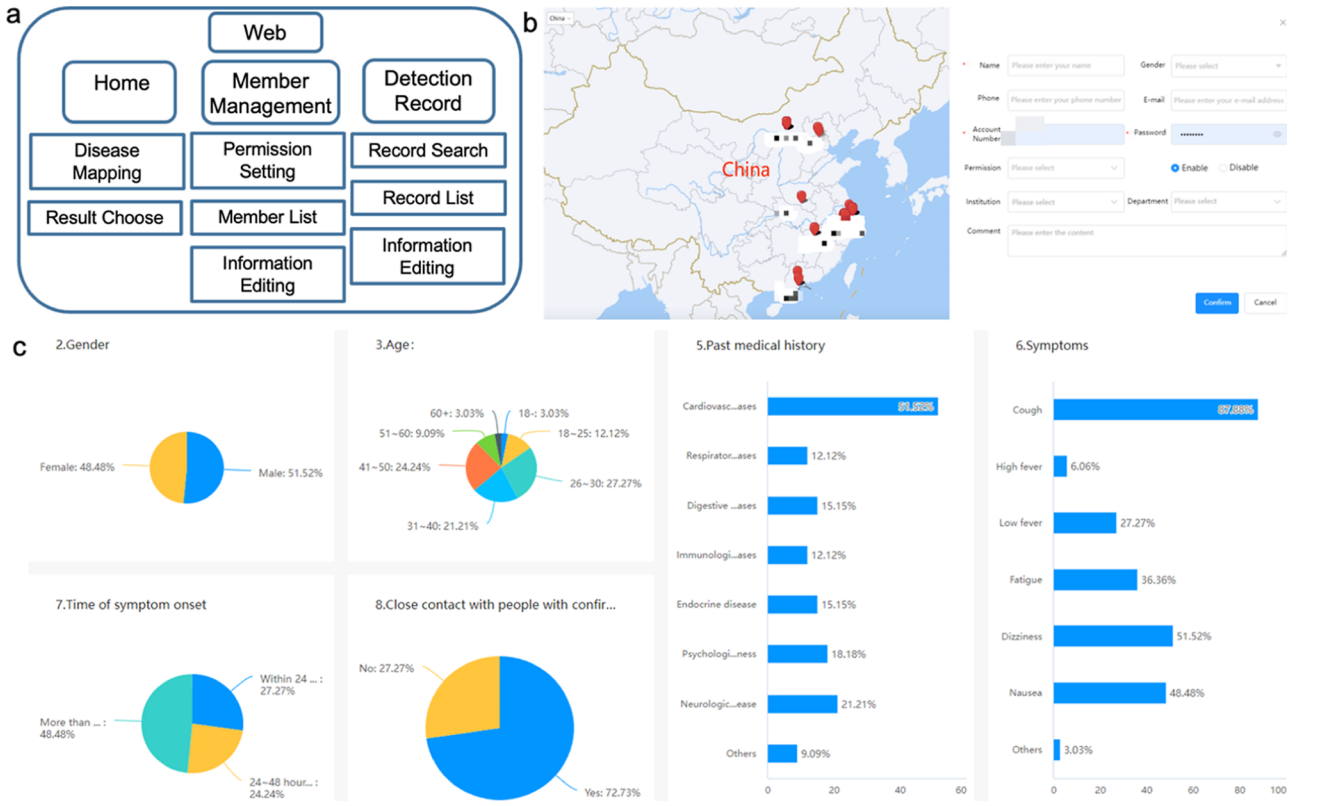

Figure 3. The diagnostic information management platform (EzDx Cloud). (a) Architecture design of the management platform back-end (server-side). (b) Screenshots of the disease mapping page and the administrator permission settings page. (c) Comprehensive analysis encompassing statistics on gender, age, past medical history, symptoms, time of symptom onset, close contact with confirmed infected persons, user location, and the correlation of these data points with test results and disease presence.

as name, gender, race, past medical history, symptoms, time of symptom onset, close contact with people with confirmed respiratory infections, and more) required for personal health information management, disease mapping, and epidemiological analysis (Figure 2b(vi)).

2.1.3. Cloud Platform. To facilitate diagnostic information management, a cloud platform was developed using the Spring Boot framework, dubbed "EzDx Cloud". Illustrated in Figure 3, the entire platform can be categorized into three essential function modules: member management module (Figure 3a), disease mapping module (Figure 3b), and statistical analysis module (Figure 3c). Member management module (Figure 3a) governs information rights for logged-in users. Users can personalize their login credentials, setting their username and password from this interface. Within disease mapping module (Figure 3b), we seamlessly associate all uploaded location data with test results, showcasing them on a map with Baidu's map API. Statistical analysis module (Figure 3c) presents all test records on disease map and personal information in a meticulously organized format. Combining it with Baidu's map API enables comprehensive disease mapping, and the gathered data proves invaluable for various medical big data analyses, including epidemiological research, epidemic tracking, and prediction. Users can access the disease mapping module via the WeChat mini-program and obtain real-time information on disease outbreaks. Upon inputting their correct mobile phone number (facilitated through an Alibaba API), users receive short message notifications containing their test results, accompanied by relevant guidance. The module features a name query function for swift access to test results. Furthermore, administrators have the capability to edit, rectify, or delete records within this module, ensuring data accuracy and integrity.

2.2. Investigating the Compatibility of Hand-Held Isothermal Fluorescence Detector with Recombinase Assisted Amplification, LAMP, and LAMP-PfAgo Assays. The detailed experimental procedures can be found in the Supporting Information and Materials and Methods.

2.3. Identifying Two Common Respiratory Viruses Combining with One-Tube/One-Step LAMP-CRISPR Assay. *2.3.1. LAMP-CRISPR Assay.* The LAMP-CRISPR Assay involves a total reaction volume of 25 μL, comprising the following components: 1× LAMP Isothermal buffer (New England Biolab, US), 1×primer mix (see Tables S1 and S2), 8U BST2.0 (SignalChem Biotech Inc., SuZhou), 24 nM Cas12b (SignalChem Biotech Inc., SuZhou), 25 nM sgRNA (refer to Tables S1 and S2), 500 nM ssDNA reporter (Tables S1 and S2), 6 mM MgSO4, and 1U AMV (Promega, US). Additionally, either 1 μL of RNA standard templates (obtained from the National Sharing Platform for Reference Materials, China) or purified virus RNA, including human nasopharyngeal swabs from real samples, is added to the reaction mixture. Further details regarding the reagents used in the LAMP-CRISPR assay can be found in Table S3. The incubation of the reaction mixture occurs in a WeD-1 system at 65 °C for 30 min.

3. RESULTS AND DISCUSSION

3.1. Automated Color Discrimination Using the WeChat Mini-Program. Although machine learning methods

https://doi.org/10.1021/acs.analchem.4c01762
Anal. Chem. 2024, 96, 13494−13503

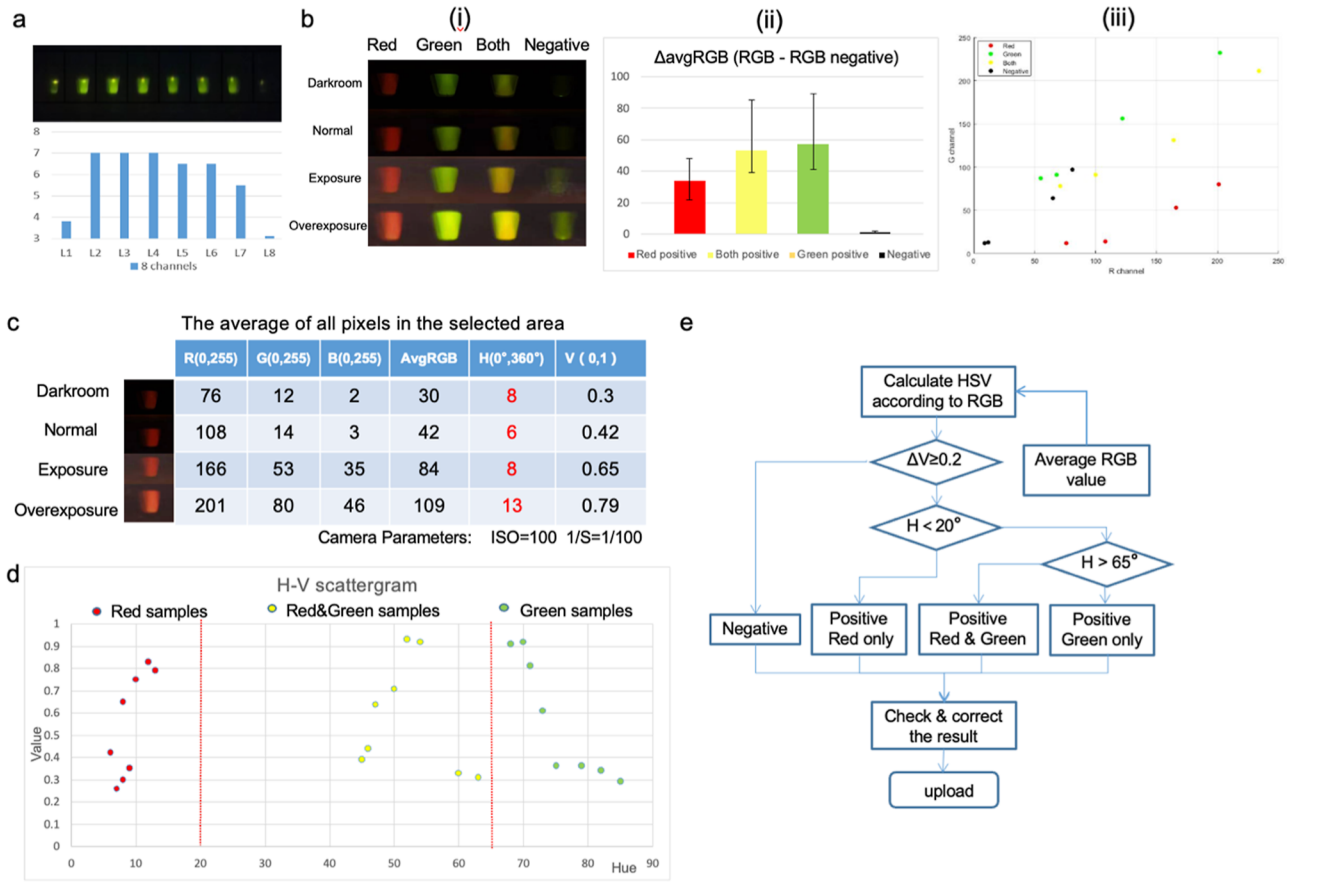

Figure 4. Automated color discrimination using the WeChat mini-program. (a) Singleplex detection based on RGB values, demonstrating image data (top) and its corresponding bar chart (bottom) showing RGB values after the negative control RGB value is subtracted from the sample image RGB value. (b) Multiplex detection based on RGB values, showcasing image data (i) alongside a corresponding bar chart (ii) that displays the RGB values for each sample after subtracting the negative control RGB value, and an R−G scatter diagram plotted with R and G values collected under different ambient light. (c) A comparison of the stability of R, G, B, averageRGB, *H*, and *V* values collected from images captured in various external light environments, showing that the *H* parameter is less influenced by external light. (d) A scatter plot of *H* and *V* values collected from images captured in various external light environments. A color differentiation method was established, utilizing the *H* angle as the domain value index. (e) The algorithm flowchart outlines the process of positive/negative judgment and target discrimination for various samples.

offer superior accuracy in discrimination, their seamless operation within the lightweight framework of mini-programs is challenging. Uploading images for evaluation on the server-side and subsequent transmission back to the user-side requires frequent network requests, causing poor compatibility and redundancy in the result judgment system. To address this issue, we opted for a client-side discrimination scheme that ensures algorithmic stability within the mini-program environment without compromising on compatibility.

The fluorescence image obtained from the reaction region is mainly composed of the fluorescence of the reactant and the ambient light reflecting off the surrounding environment. Interpretation of the fluorescence image is subject to various factors, such as numerical fluctuations resulting from systematic error and changes in ambient light. By subtracting the sample image RGB value from the negative control, we can significantly reduce the impact of external light or camera system errors. By adopting this approach, we can effectively distinguish between negative and positive samples in both singleplex and multiplex detection, as demonstrated in Figure 4a,b(i), and b(ii). However, RGB is a device-specific parameter that can vary greatly under the influence of external light, making it difficult to set accurate thresholds for distinguishing fluorescence colors (Figure 4b(iii)). To ensure greater precision and robustness when recognizing multiple targets, a more suitable color space and discrimination algorithm is necessary.

To address this issue, we have implemented the more descriptive HSV color space, which consists of three components: *H* (Hue), *S* (Saturation), and *V* (Value). In this context, H typically represents the color type, S denotes color purity, and *V* signifies brightness. The conversion formulas for RGB to HSV are as follows

$$h = \begin{cases} 0^\circ, & \max = \min \\ 60^\circ \times \dfrac{g - b}{\max - \min} + 0^\circ, & \max = r,\ g \geq b \\ 60^\circ \times \dfrac{g - b}{\max - \min} + 360^\circ, & \max = r,\ g < b \\ 60^\circ \times \dfrac{g - b}{\max - \min} + 120^\circ, & \max = g \\ 60^\circ \times \dfrac{g - b}{\max - \min} + 240^\circ, & \max = b \end{cases}$$

https://doi.org/10.1021/acs.analchem.4c01762
Anal. Chem. 2024, 96, 13494−13503

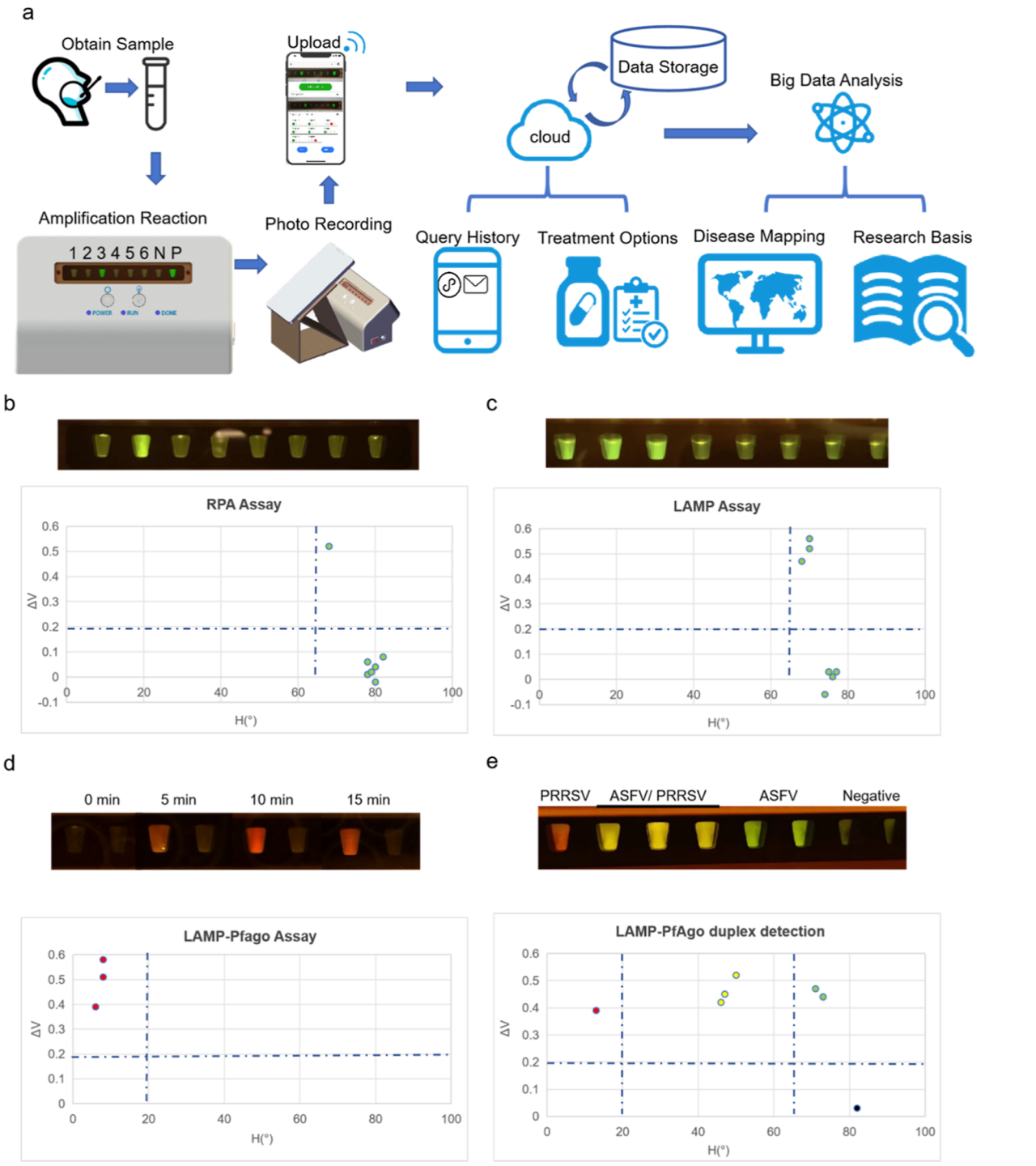

Figure 5. Assessing Platform Compatibility: (a) workflow of the IoT molecular diagnostic device detection system for detecting Common Respiratory pathogens. Detection and discrimination of various targets using the WeChat mini-program with Different Assays: (b) RAA Assay for SARS-CoV-2 detection in patient samples, (c) LAMP Assay for SARS-CoV-2 detection in patient samples, (d) LAMP-PfAgo assay for detecting ASFV, and (e) LAMP-PfAgo assay for duplex detection of PRRSV and ASFV. Evaluation conducted with 100 copies/reaction of PRRSV RNA and ASFV DNA.

$$s = \begin{cases} 0 & \max = 0 \\ \dfrac{\max - \min}{\max} = 1 - \dfrac{\min}{\max}, & \max \neq 0 \end{cases}$$

$$v = \max$$

By taking images with the same experiment result at different external light environments (Figure 4b(i),c), we compared R, G, B, averageRGB, H, and V values. As shown in Figure 4c, this parameter H value is less influenced by external light and maintains strong stability compared to the RGB values and V values, despite these changes in external environment. It is crucial to maintain the original color value of the sample in order to enable the H angle to be in the most distinguishable state without causing any shifts in color. Hence, we utilize the HSV color space to distinguish between different targets, as

https://doi.org/10.1021/acs.analchem.4c01762
Anal. Chem. 2024, 96, 13494−13503

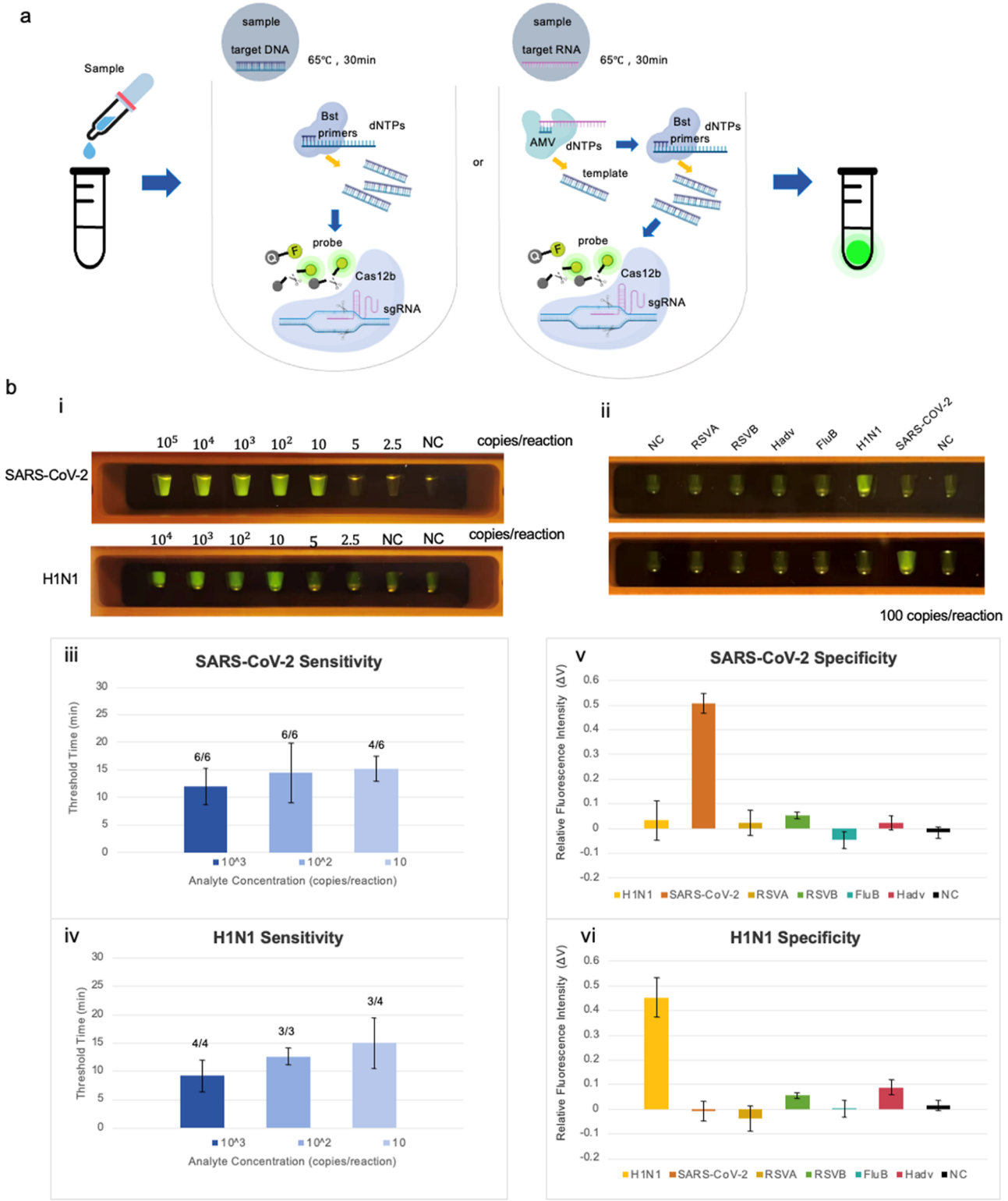

Figure 6. Comprehensive analysis of one-tube/one-step LAMP-CRISPR Assay for respiratory virus identification. (a) Illustration of the mechanism underlying the LAMP-CRISPR assay. (b) Sensitivity and specificity evaluation of IoT molecular diagnostic device/LAMP-CRISPR system. Subsections: (i) visual representation of results from Table S4, (ii) visual demonstration of results in (b(v),(vi)), (iii) mean and standard deviation of SARS-CoV-2 RNA threshold times, (iv) mean and standard deviation of H1N1 RNA threshold times, (v) specificity assessment for SARS-CoV-2 detection using 100 copies of H1N1 RNA, SARS-CoV-2 RNA, RSVA RNA, RSVB RNA, Flu B RNA, and HAdV DNA, and (vi) specificity evaluation for H1N1 detection using 100 copies of H1N1 RNA, SARS-CoV-2 RNA, RSVA RNA, RSVB RNA, Flu B RNA, and HAdV DNA. Experiments were quintuply repeated for reproducibility and consistency.

well as to discriminate between negative and positive samples but we choose to use Value.

The substantial difference in *H* angles between red and green hues ensures clearer and more distinguishable results.

https://doi.org/10.1021/acs.analchem.4c01762
Anal. Chem. 2024, 96, 13494−13503

Our detection system can excite different fluorophores to generate distinct fluorescence colors. Consequently, we have chosen green fluorophores, like FAM, and red fluorophores, such as R_{ox}, to achieve optimal contrast in multiplex detection.

We performed multiplex detection for two sets of tests with identical experimental conditions. We collected image data in four different external lighting environments (Figure 4b(i)). Ultimately, we determined a color distinction method using the H angle as the domain value index (Figure 4d). The algorithm flowchart for positive/negative judgment and target discrimination is detailed and illustrated in Figure 4e. First, RGB data is collected from the selected region of the image and the average RGB value is computed. Next, the RGB value is converted to HSV color space and the original V value of the sample is subtracted from the V value of the negative control group. We utilize the resulting ΔV value to determine the negative or positive status of a sample (Figure 4e). To achieve this, a threshold ΔV value of 0.2 is predetermined based on a large number of tests and statistical analysis. Afterward, positive samples undergo additional classification, as illustrated in Figure 4d,e, based on the defined threshold H value (20 and 65°), established through rigorous testing and statistical analysis. This step aids in pinpointing the specific target present in the sample. In instances of suboptimal image quality that might lead to inaccurate assessments, our system provides the flexibility for manual correction of results (Figures 2b(v) and 4e). The corrected outcomes can subsequently be uploaded to our information management platform for accurate record-keeping.

3.2. Versatile Compatibility of the Platform: Supporting Various Assays and Applications for Different Targets. We recently demonstrated the compatibility of the hand-held isothermal fluorescence detector with LAMP-PfAgo assay, showcasing its effectiveness in duplex visualization of aquatic pathogens.[27] In this study, we integrated the newly developed WeChat mini-program with the hand-held isothermal fluorescence detector, thereby creating an IoT molecular diagnostic device detection system (Figure 5a). We further investigated the device's versatility by assessing its performance across diverse isothermal nucleic acid detection assays that require varying operating temperatures and exhibit a range of fluorescence intensities. Additionally, we evaluated the compatibility of the device for various virus detection and tested its effectiveness in detecting samples from patients exhibiting respiratory disease symptoms. Specifically, we evaluated its efficacy with recombinase assisted amplification (RAA) at 39 °C (Figure 5b), LAMP at 65 °C (Figure 5c), and LAMP-PfAgo assays covering a temperature range from 65 to 95 °C (Figure 5d,e). Notably, Figure 5d,e demonstrate the device's remarkable capability in facilitating PfAgo cleavage even at the high temperature of 95 °C.

In Figure 5a and Video S1, we present the workflow of the IoT molecular diagnostic device detection system. For SARS-CoV-2 detection, oral swab samples were collected, as depicted in Figures 5a and S1. Despite RAA emitting relatively low fluorescence intensity, real sample testing with the WeChat mini-program for automated color discrimination revealed one positive SARS-CoV-2 case out of eight patients exhibiting respiratory disease symptoms (Figure 5b). This positive result contradicted the negative outcome from the Antigen test (Figure S2a). Similarly, with LAMP, we detected three positive SARS-CoV-2 cases out of 8 patients (Figure 5c and Video S1), though one of these positive samples returned negative on the Antigen test (Figure S2b). Additionally, Figure 5e illustrates the device's capability to provide dual fluorescence channels, enabling the duplex detection and discrimination of both African Swine Fever Virus (ASFV) and Porcine Reproductive and Respiratory Syndrome Virus (PRRSV) using the WeChat mini-program. Concurrently, the results were forwarded to our "EzDx Cloud" for health management, treatment guidance analysis, and disease mapping. Patients also received short message notifications containing their test results, as shown in Video S1.

3.3. Identifying Two Common Respiratory Viruses Combining with One-Tube/One-Step LAMP-CRISPR Assay. Recently, some one-tube, one-step LAMP-CRISPR-Cas assays have emerged. However, despite the convenience offered by this approach, compatibility between LAMP amplification (optimal working temperature 63−65 °C) and CRISPR-specific cleavage (optimal working temperature < 60 °C) remains an issue,[28] given their different working temperatures and the potential for interference with amplification due to cleavage. While some groups have tackled this problem by using suboptimal PAM or protospacer-adjacent motif-interacting domain engineered Cas12b to reduce interference,[29] we have taken a unique approach. Our study introduces a novel solution, which improves compatibility between LAMP amplification and CRISPR-specific cleavage through leveraging a newly discovered thermostable CRISPR-Cas12b variant to maintain LAMP's Bst polymerase at its optimal temperature of 63−65 °C (Figure 6a).[30] We have pioneered a novel one-tube/one-step LAMP-CRISPR-Cas assay tailored for detecting two common respiratory viruses. This innovative assay demonstrates significantly improved compatibility between LAMP amplification and CRISPR-specific cleavage within a single reaction.

SARS-CoV-2 and H1N1 are prevalent respiratory viruses with overlapping clinical presentations. The swift and accurate differentiation and diagnosis of these viruses, whether in community or outpatient settings, are imperative for guiding appropriate treatment strategies. In Figures 6b and S3, we present the effectiveness of our newly developed one-tube/one-step LAMP-CRISPR-Cas assay for detecting both viral targets. Our device exhibits exceptional sensitivity, capable of detecting as few as 10 copies of SARS-CoV-2 RNA (4/6) and 10 copies of H1N1 RNA (3/4) (Figure 6b(i)). Moreover, it reliably identifies 100 copies of SARS-CoV-2 RNA and 100 copies of H1N1 RNA and more than this copies of targets with impeccable repeatability (Figure 6b(iii,iv)) and specificity (Figure 6b(v,vi)). Furthermore, leveraging the automated color discrimination feature of the WeChat mini-program, the IoT molecular diagnostic device/LAMP-CRISPR detection system exhibited 100% consistency in detecting SARS-CoV-2 and H1N1 compared to the qPCR instrument/LAMP-CRISPR (Table S4), underscoring the device's robust performance in identifying prevalent respiratory viruses.

4. CONCLUSION

In summary, we have developed an innovative IoT molecular diagnostic device that features a WeChat mini-program and is designed for the simultaneous detection and spatiotemporal mapping of respiratory pathogens. Our findings emphasize the platform's versatility in accommodating assays that operate at different temperatures and emit varied fluorescence intensities. Additionally, they underscore the superior sensitivity of rapid nucleic acid detection methods in comparison to antigen tests.

https://doi.org/10.1021/acs.analchem.4c01762
Anal. Chem. 2024, 96, 13494−13503

Furthermore, our results highlight the clinical efficacy of the diagnostic system, particularly in enhancing personal health management through the Internet of Medical Things (IoMT). Notably, our device has demonstrated high sensitivity and specificity through the integration of the one-tube/one-step LAMP-CRISPR method, which utilizes a newly discovered thermophilic Cas12b protein.

Compared to prior studies, our WeChat mini-program enabled IoT detection system offers several distinct advantages. First, our device operates via a mini-program, eliminating the need for app downloading and installations, facilitating instant data sharing, and allowing rapid dissemination of the epidemic situation through social software, making it easier to access testee information for epidemiological analysis. Additionally, our device seamlessly integrates with traditional consumables while delivering precise and fast molecular diagnosis at a remarkably low cost, making it more accessible to the general public.

Looking ahead, this diagnostic system, combined with EzDx Cloud, holds immense potential for monitoring and early warning of infectious diseases in both human and animal populations. With its user-friendly interface and seamless integration with traditional consumables, the system promises widespread application in the surveillance and management of sensitive diseases.

■ ASSOCIATED CONTENT

Supporting Information

The Supporting Information is available free of charge at https://pubs.acs.org/doi/10.1021/acs.analchem.4c01762.

Workflow of the IoT molecular diagnostic device detection system (MP4)

Detailed experimental procedures for RAA, LAMP, and LAMP-PfAgo assays, primer and sgRNA design, and additional experimental data (PDF)

■ AUTHOR INFORMATION

Corresponding Author

Jinzhao Song − *Hangzhou Institute of Medicine, Zhejiang Cancer Hospital, Chinese Academy of Sciences, Hangzhou, Zhejiang 310022, China;* orcid.org/0000-0002-2097-8685; Email: songjinzhao@ucas.ac.cn

Authors

Kaizheng Wang − *Academy of Medical Engineering and Translational Medicine, Medical College, Tianjin University, Tianjin 300072, China; Hangzhou Institute of Medicine, Zhejiang Cancer Hospital, Chinese Academy of Sciences, Hangzhou, Zhejiang 310022, China*

Tao Zhang − *Academy of Medical Engineering and Translational Medicine, Medical College, Tianjin University, Tianjin 300072, China; Hangzhou Institute of Medicine, Zhejiang Cancer Hospital, Chinese Academy of Sciences, Hangzhou, Zhejiang 310022, China*

Tianjiao Jiao − *Hangzhou Institute of Medicine, Zhejiang Cancer Hospital, Chinese Academy of Sciences, Hangzhou, Zhejiang 310022, China; School of Molecular Medicine, Hangzhou Institute for Advanced Study, University of the Chinese Academy of Sciences, Hangzhou, Zhejiang 310024, China*

Feibiao Pang − *Hangzhou EzDx Technology Co., Ltd., Hangzhou, Zhejiang 311231, China*

Fengyi Dai − *Academy of Medical Engineering and Translational Medicine, Medical College, Tianjin University, Tianjin 300072, China; Hangzhou Institute of Medicine, Zhejiang Cancer Hospital, Chinese Academy of Sciences, Hangzhou, Zhejiang 310022, China*

Zhanfang Zhang − *Academy of Medical Engineering and Translational Medicine, Medical College, Tianjin University, Tianjin 300072, China; Hangzhou Institute of Medicine, Zhejiang Cancer Hospital, Chinese Academy of Sciences, Hangzhou, Zhejiang 310022, China*

Xiang Li − *Hangzhou Institute of Medicine, Zhejiang Cancer Hospital, Chinese Academy of Sciences, Hangzhou, Zhejiang 310022, China; School of Molecular Medicine, Hangzhou Institute for Advanced Study, University of the Chinese Academy of Sciences, Hangzhou, Zhejiang 310024, China*

Yao Chen − *Hangzhou Institute of Medicine, Zhejiang Cancer Hospital, Chinese Academy of Sciences, Hangzhou, Zhejiang 310022, China*

Hongyu Zhang − *Hangzhou Institute of Medicine, Zhejiang Cancer Hospital, Chinese Academy of Sciences, Hangzhou, Zhejiang 310022, China*

Zhiguang Chen − *Hangzhou EzDx Technology Co., Ltd., Hangzhou, Zhejiang 311231, China*

Complete contact information is available at: https://pubs.acs.org/10.1021/acs.analchem.4c01762

Notes

The authors declare no competing financial interest.

J.S., F.P., F.D., K.W., and T.J. are coinventors on a patent related to this manuscript (application number, CN202210983377.8A, applied August 16, 2022; international application number, PCT/CN2023/109464, applied July 27, 2023; Publication/Patent Number: CN218860746U, granted April 14, 2023).

■ ACKNOWLEDGMENTS

This study was supported by the National Key Research and Development Program of China (2023YFD2402100) and Zhejiang Leading Innovation and Entrepreneurship Team Program (2022R01006).

■ REFERENCES

(1) Caliendo, A. M.; Gilbert, D. N.; Ginocchio, C. C.; Hanson, K. E.; May, L.; Quinn, T. C.; Tenover, F. C.; Alland, D.; Blaschke, A. J.; Bonomo, R. A.; et al. *Clin. Infect. Dis.* **2013**, *57* (Suppl 3), S139−S170.

(2) Haldane, V.; De Foo, C.; Abdalla, S. M.; Jung, A. S.; Tan, M.; Wu, S.; Chua, A.; Verma, M.; Shrestha, P.; Singh, S.; et al. *Nat. Med.* **2021**, *27* (6), 964−980.

(3) Mistry, P.; Barmania, F.; Mellet, J.; Peta, K.; Strydom, A.; Viljoen, I. M.; James, W.; Gordon, S.; Pepper, M. S. *Front. Immunol.* **2022**, *12*, 809244.

(4) Raina, S. K.; Kumar, R. *J. Fam. Med. Prim. Care* **2022**, *11* (5), 1595−1597.

(5) Jorquera, P. A.; Tripp, R. A. *Expert Rev. Respir. Med.* **2017**, *11* (8), 609−615.

(6) Kajon, A., 3rd; Lynch, J., III *Semin. Respir. Crit. Care Med.* **2016**, *37* (04), 586−602.

(7) Najjar-Debbiny, R.; Gronich, N.; Weber, G.; Khoury, J.; Amar, M.; Stein, N.; Goldstein, L. H.; Saliba, W. *Clin. Infect. Dis.* **2023**, *76* (3), e342−e349.

(8) Kawai, N.; Ikematsu, H.; Iwaki, N.; Maeda, T.; Kanazawa, H.; Kawashima, T.; Tanaka, O.; Yamauchi, S.; Kawamura, K.; Nagai, T.; et al. *J. Infect.* **2008**, *56* (1), 51−57.

(9) Dou, L.; Reynolds, D.; Wallace, L.; O'Horo, J.; Kashyap, R.; Gajic, O.; Yadav, H. *Mayo Clin. Proc.* **2020**, *4* (2), 176−182.
(10) Heinonen, S.; Silvennoinen, H.; Lehtinen, P.; Vainionpaa, R.; Vahlberg, T.; Ziegler, T.; Ikonen, N.; Puhakka, T.; Heikkinen, T. *Clin. Infect. Dis.* **2010**, *51* (8), 887−894.
(11) Jean, S.; Burnham, C. A. D.; Chapin, K.; Garner, O. B.; Pant Pai, N.; Turabelidze, G.; Butler-Wu, S. *Clin. Chem.* **2021**, *68* (1), 19−26.
(12) Alemi, F.; Vang, J.; Bagais, W. H.; Guralnik, E.; Wojtusiak, J.; Moeller, F. G.; Schilling, J.; Peterson, R.; Roess, A.; Jain, P. *Qual. Manag. Health Care* **2023**, *32* (Supplement1), S11−S20.
(13) Rader, B.; Gertz, A.; Iuliano, A. D.; Gilmer, M.; Wronski, L.; Astley, C. M.; Sewalk, K.; Varrelman, T. J.; Cohen, J.; Parikh, R.; et al. *MMWR Morb Mortal Wkly. Rep.* **2022**, *71*, 489−494.
(14) Dolgin, E. *Mar 21. Online ahead of print. Nature* **2024**.
(15) Kok, J.; Blyth, C. C.; Foo, H.; Patterson, J.; Taylor, J.; McPhie, K.; Ratnamohan, V. M.; Iredell, J. R.; Dwyer, D. E. *J. Clin. Microbiol.* **2010**, *48* (1), 290−291.
(16) Yuce, M.; Filiztekin, E.; Ozkaya, K. G. *Biosens. Bioelectron.* **2021**, *172*, 112752.
(17) Klajmon, A.; Olechowska-Jarzab, A.; Salamon, D.; Sroka-Oleksiak, A.; Brzychczy-Wloch, M.; Gosiewski, T. *Viruses* **2021**, *14* (1), 17.
(18) Song, J.; Pandian, V.; Mauk, M. G.; Bau, H. H.; Cherry, S.; Tisi, L. C.; Liu, C. *Anal. Chem.* **2018**, *90* (7), 4823−4831.
(19) Song, J.; Liu, C.; Mauk, M. G.; Peng, J.; Schoenfeld, T.; Bau, H. H. *Anal. Chem.* **2018**, *90* (2), 1209−1216.
(20) Song, J.; Liu, C.; Mauk, M. G.; Rankin, S. C.; Lok, J. B.; Greenberg, R. M.; Bau, H. H. *Clin. Chem.* **2017**, *63* (3), 714−722.
(21) Song, J.; Mauk, M. G.; Hackett, B. A.; Cherry, S.; Bau, H. H.; Liu, C. *Anal. Chem.* **2016**, *88* (14), 7289−7294.
(22) Chen, J.; Qiu, T.; Mauk, M. G.; Su, Z.; Fan, Y.; Yuan, D. J.; Zhou, Q.; Qiao, Y.; Bau, H. H.; Ying, J.; et al. *Chin. Chem. Lett.* **2022**, *33* (8), 4126−4132.
(23) Huang, H. S.; Tsai, C. L.; Chang, J.; Hsu, T. C.; Lin, S.; Lee, C. C. *Clin. Microbiol. Infect.* **2018**, *24* (10), 1055−1063.
(24) Babady, N. E. *Expert Rev. Mol. Diagn.* **2013**, *13* (8), 779−788.
(25) Denkinger, C. M.; Schumacher, S. G.; Boehme, C. C.; Dendukuri, N.; Pai, M.; Steingart, K. R. *Eur. Respir. J.* **2014**, *44* (2), 435−446.
(26) Zahavi, M.; Rohana, H.; Azrad, M.; Shinberg, B.; Peretz, A. *Diagnostics* **2022**, *12* (8), 1877.
(27) Pang, F.; Zhang, T.; Dai, F.; Wang, K.; Jiao, T.; Zhang, Z.; Zhang, L.; Liu, M.; Hu, P.; Song, J. *Biosens. Bioelectron.* **2024**, *254*, 116187.
(28) Li, L.; Li, S.; Wu, N.; Wu, J.; Wang, G.; Zhao, G.; Wang, J. *ACS Synth. Biol.* **2019**, *8* (10), 2228−2237.
(29) Tong, X.; Zhang, K.; Han, Y.; Li, T.; Duan, M.; Ji, R.; Wang, X.; Zhou, X.; Zhang, Y.; Yin, H. *Nat. Chem. Biol.* **2024**, *20*, 885−893.
(30) Dai, F.; Pang, F.; Jiao, T.; Wang, K.; Wang, Z.; Zhang, Z.; Pei, L.; Xiang, L.; Chen, Y.; Chen, Z.; Song, J. A Compact, Palm-Sized Isothermal Fluorescent Diagnostic Device for Personal Health Monitoring and Beyond via One-Tube/One-Step LAMP-CRISPR Assay. **2024**, under review.

https://doi.org/10.1021/acs.analchem.4c01762
Anal. Chem. 2024, 96, 13494−13503